

Development Of A MEMS Vibratory Gyroscope Using High-Order Continuous-Time Band-Pass Sigma-Delta Modulator

Reshma Jayaprakash, P.K. Senthil Kumar

Abstract

This work describes about the design and implementation of a double closed-loop control system for MEMS vibratory gyroscope using sixth-order and eighth-order continuous time band-pass sigma-delta modulator. A gyroscope is a device based on the principles of angular momentum for measuring the orientation. MEMS (Micro-electro-mechanical Systems) refer to devices or systems integrated with electrical and mechanical components in the scale of microns. There are two orthogonal modes: drive and sense mode, and these modes has corresponding control loops. The sense mode is controlled by sixth-order continuous- time force-feedback band-pass sigma-delta modulator. Here we choose the band-pass sigma-delta modulator so that only less sampling frequency is required. The principle of operation is based on Coriolis force, it transfers energy from drive mode to sense mode. By giving the input angular rate, the proof mass displacement and Coriolis force takes place. Delta-sigma ($\Delta\Sigma$) or sigma-delta($\Sigma\Delta$) modulation is a digital signal processing, or DSP method for converting analog signals into digital signals as found in an ADC. It is also used to move higher-resolution digital signals into lower-resolution digital signals as part of the process to convert digital signals into analog. By using this double closed-loop control system, the bandwidth and linearity is maintained. The parameters of both control loops can be optimized by genetic algorithm (GA) as a future work.

Index Terms— MEMS, gyroscope, sigma-delta modulator, bandpass, genetic algorithm (GA)

I. INTRODUCTION

Micro-electro-mechanical-system (MEMS) vibratory gyroscopes. It is based on Coriolis force. The Coriolis Effect is a deflection of moving objects when they are viewed in a rotating reference frame. There are two orthogonal vibration modes: drive and sense mode, with two corresponding control loops. The topology of gyroscope

L3GD20 has been designed. Sense mode is controlled by a sixth-order continuous-time force-feedback band-pass sigma-delta modulator (BP- $\Sigma\Delta$ M). Genetic algorithm is used for the optimization of double closed loop control system. The operation principle of the vibratory gyroscope is the transfer of energy between the drive mode and the sense mode caused by Coriolis acceleration [1,2]; the output signal is amplitude modulated at the drive frequency. The sensing element should be in high sensitivity so that to increase the sensitivity, the quality factor of the sensing element must be high. A high-order bandpass sigma-delta modulator can provide better noise shaping than the second-order. A low-pass $\Sigma\Delta$ M requires high sampling frequency. Here the sense mode is controlled by a sixth-order continuous-time band-pass $\Sigma\Delta$ M.

Mapping the sense mode of a MEMS vibratory gyroscope in a high-order sigma-delta modulator gives many advantages like increased bias stability, linearity and direct digital output [3-11]. A sigma-delta modulator of closed-loop control systems are striking due to the fact that force feedback can increase the linearity, bandwidth, dynamic range of the sensor. Yufeng Dong et al described a micromachined vibratory gyroscopes controlled by a high-order bandpass sigma-delta modulator [9]. So far, most systems are designed using low-pass $\Sigma\Delta$ M. The output characteristics of vibratory gyroscopes are narrowband amplitude modulated signal. Since, a bandpass $\Sigma\Delta$ M is more applicable than lowpass $\Sigma\Delta$ M [9]. J. Raman et al described a closed-loop digitally controlled MEMS gyroscope with unconstrained sigma-delta force-feedback [10]. This work report structural design and model measurement of a MEMS gyroscope system with a resolution of $0.025^\circ/\text{s}/\sqrt{\text{Hz}}$. The design makes wide use of control loops, the two modes; primary and secondary. The amplitude and resonance frequency are tracked and controlled. In a fourth-order low-pass $\Sigma\Delta$ M [3,4]; two electronic integrators were cascaded whereas in the case of a bandpass $\Sigma\Delta$ M, the sensing element were cascaded with electronic resonators. Rodjégard et al described a digitally controlled MEMS gyroscope with 3.2 deg/Hr stability [7], operated in vacuum using fifth-order low-pass $\Sigma\Delta$ M. These architectures all requires high sampling frequency compared to the bandwidth of the gyroscope. As reported in [9] electronic integrators of a low-pass $\Sigma\Delta$ M are replaced by electronic resonators. The sampling frequency of the bandpass $\Sigma\Delta$ M control system can be reduced by the complex pairs of zeros generated in the quantization noise transfer function (QNTF) of the closed loop system. It produces notches in the frequency response further controlling quantization noise. Power dissipation of the interface electronics can be reduced by the low sampling frequency. The work described in [11] implemented a sixth-order bandpass continuous-time $\Sigma\Delta$ M in a PCB circuit. The power spectral density (PSD) of the output bitstream attained a noise floor of $-90\text{dBV}/\text{Hz}^{1/2}$.

Work represented in this paper explains about the performance of the gyroscope, the sense mode is controlled by the sixth-order continuous-time band-pass $\Sigma\Delta$ M using two digital to analogue converters (DACs); half return zero (HRZ) and return zero (RZ) [12] and also without using DACs. The input angular rate is converted to 16 bit integer by adding a scale factor. The design is implemented in two different methods, and the design of eighth-order bandpass $\Sigma\Delta$ M is also shown as a future work. In order to enhance the output of the design optimization [13,14] can be

done using genetic algorithm (GA) and Monte Carlo simulation. The goal for optimizing is to minimize the proof mass displacement in the sense mode, maximize the signal noise ratio (SNR) of the output bitstream and to minimize the settling time of the self-oscillation in the drive mode. The model is designed using MATLAB Simulink.

II. SENSE MODE AND DRIVE MODE CONTROL LOOPS

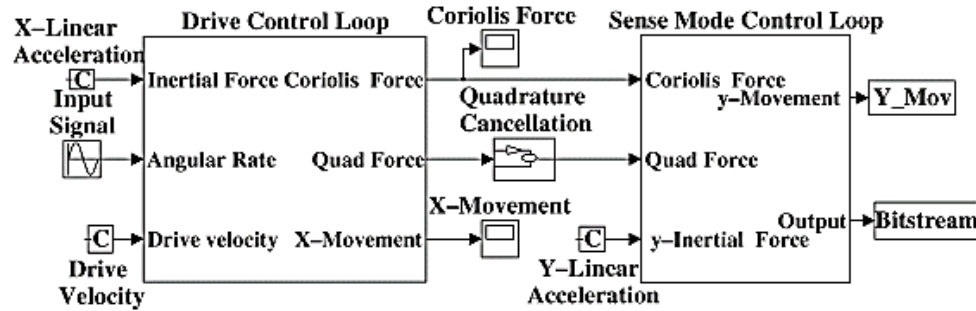


Fig. 1. Block diagram representation of sense mode and drive mode

Fig. 1 shows a block diagram of a closed-loop control system of vibratory gyroscope. It consists of a drive mode and sense mode control loops. The drive mode control-loop is shown in fig. 2.

A. Drive Mode Control-Loop

The main function of the drive mode control loop is to keep the drive oscillation at constant amplitude (X_0) and frequency (w_x). The transfer function of the sensing element in the sense direction is given by,

$$M_m(s) = \frac{1}{ms^2 + bs + k} = \frac{1/m}{s^2 + \frac{w_y}{Q_y}s + w_y^2} \quad (1)$$

Where m is the mass of the sensing element, b is the damping coefficient, k is the spring stiffness, $w_y = \sqrt{k/m}$ is the resonant frequency, and $Q_y = \sqrt{mk}/b$ is the quality factor of the sense mode. Vibrating proof mass motion can be described as $x = X_0 \sin(w_x t)$. The Coriolis force is acted on y -axis when the sensor is rotated around the z -axis with an angular rate Ω_z . Coriolis force is given by,

$$F_{\text{coriolis}} = 2m \frac{dx}{dt} \Omega_z = 2mX_0w_x \Omega_z \cos(w_x t). \quad (2)$$

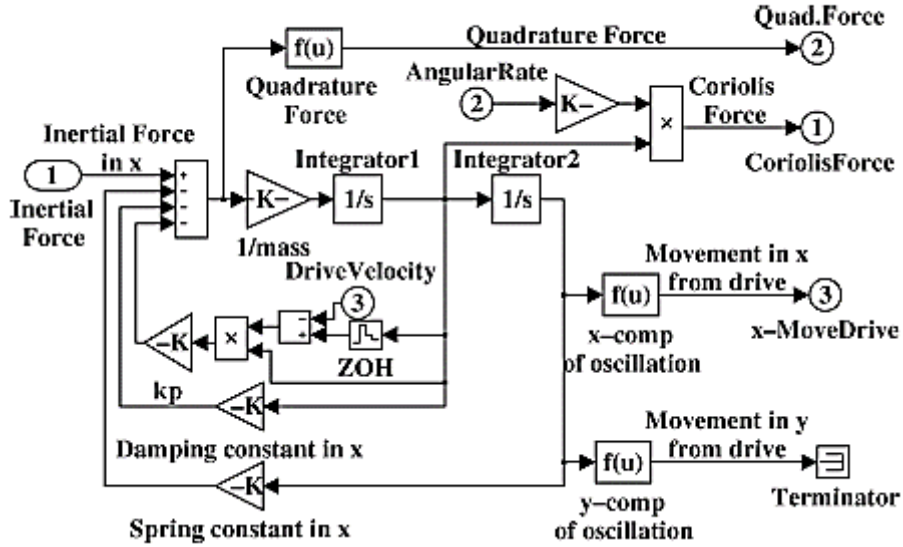


Fig. 2. Design of a drive mode control loop

B. Sixth-Order Continuous-time Band-pass Sigma-delta Modulator using DACs

The block diagram shown in fig. 3 represents Simulink model of a sixth-order continuous-time band-pass electromechanical sigma-delta modulator for the sense mode control loop. The sensor is represented by a transfer function as given in equation (1). The architecture includes a pick off circuit with gain K_{po} , boost amplification with gain K_{bst} , compensator, local feedbacks of gains $K_{f1}, K_{f2}, K_{f3}, K_{f4}$, 1 bit quantizer, zero-order-hold and electrostatic force feedback arrangement. The mechanical parameters are listed in Table 1.

TABLE I PARAMETERS OF GYROSCOPE

Parameter	Drive Mode	Sense Mode
Mass of proof mass	2×10^{-9} kg	2×10^{-9} kg
Quality Factor	119	114
Resonance Frequency	4.304 kHz	4.338 kHz
Input angular rate signal frequency	2^7 Hz	2^7 Hz
Maximum input angular rate	100 deg/sec	100 deg/sec

The proof mass is activated by electrostatic driving force $F_d(t)$ along x-direction (drive mode). Thus electrostatic driving force can be written as,

$$F_d(t) = F_0 \cos \omega_d t \quad (3)$$

Where, F_0 is the constant driving force and w_d is the driving frequency. When the object rotates around the z-axis with an angular velocity of Ω_z , thus the Coriolis force is acted upon the y-axis. Therefore the system is driven into vibration in the y-axis with a frequency of w_y .

A mass (m) with velocity $v(t)$ along x-direction with an angular rate along z-axis will experience a Coriolis force along the y-direction. It is given as,

$$F_c(t) = 2mv(t) \Omega_z \tag{4}$$

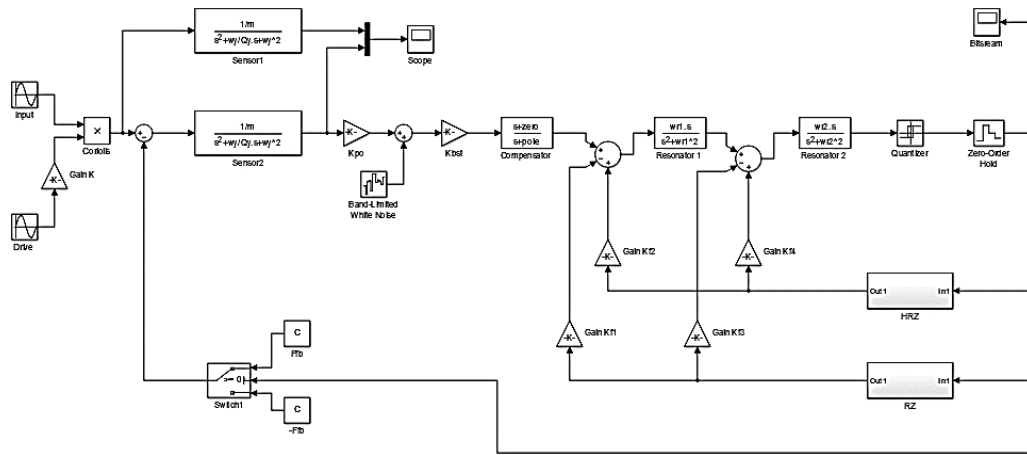


Fig. 3. Topology of a sixth-order continuous-time force feedback band-pass sigma-delta modulator

An electrostatic force feedback circuit is designed in the sigma-delta modulator. The electrostatic force is based on columbia law. It can be represented as,

$$F = \frac{q_1 q_2}{4\pi\epsilon_0 r^2} \tag{5}$$

$q_1 q_2$ are two charges and ϵ_0 is an electric constant. Electrostatic force is directly proportional to the product of two charges and inversely proportional to

$$\epsilon_0 = 8.854 \times 10^{-12} \text{F/m}$$

Electronic resonators can be described as,

$$R_1(s) = R_2(s) = k_{res} \frac{s w_y}{s^2 + w_y^2} \tag{6}$$

Transfer functions of different noises are signal transfer function (STF),

electronic noise transfer function (ENTF) and quantization noise transfer function (QNTF) [10]. These transfer functions can be described as,

$$\text{STF}(s) = \frac{2mw_x M(s) C_p(s) R_1(s) R_2(s) K_{bst} K_{po} K_q}{1+L(s)} \quad (7)$$

$$\text{ENTF}(s) = \frac{C_p(s) R_1(s) R_2(s) K_{bst} K_q}{1+L(s)} \quad (8)$$

$$\text{QNTF}(s) = \frac{1}{1+L(s)} \quad (9)$$

$$L(s) = K_q [R_2(s)(K_{f3} - K_{f4}) + \prod_{i=1}^2 R_i(s)(K_{f1} - K_{f2}) + M(s)C_p(s) \prod_{i=1}^2 R_i(s)K_{bst}K_{po}] \quad (10)$$

Two DAC's are used in the sense mode control-loop; Half return zero (HRZ) and return zero (RZ). For the conversion from proof mass displacement to voltage, pick-off circuit is used with gain k_{po} and boost gain k_{bst} and four local feedback gains are used for HRZ and RZ.

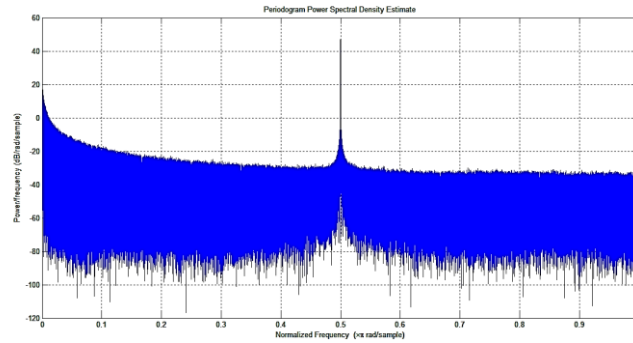


Fig. 4. Output waveform of force feedback HRZ and RZ

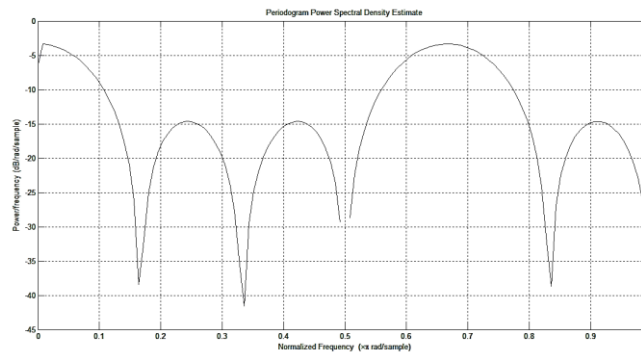


Fig. 5. Bitstream output of the sigma-delta modulator

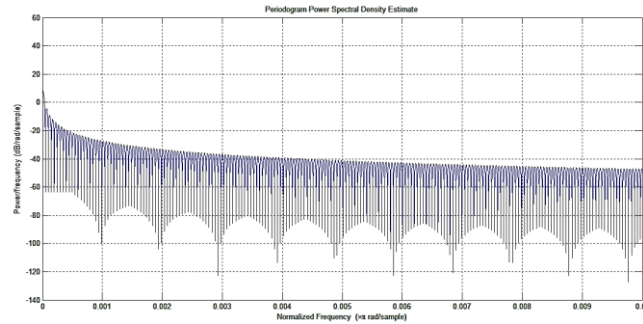


Fig. 6. Force feedback loop output

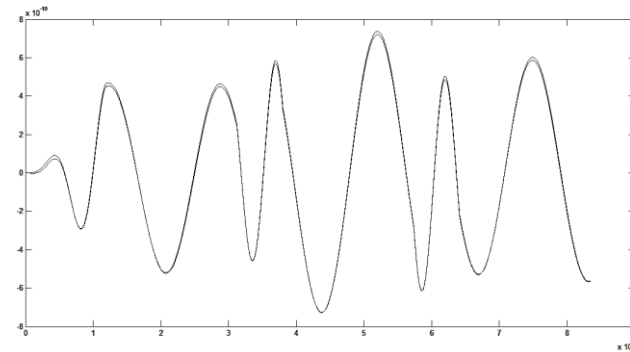


Fig. 7. Sensor output of sigma-delta modulator

C. Sixth-order Continuous-time Band-pass Sigma-delta Modulator without using DACs

Here we can see the architecture of the MEMS motion sensor L3GD20. It is a low power three axis angular rate sensor. The input is in angular rate and the output is in counts; 16 bit integer. In order to convert angular rate to counts a gain is added which is a scale factor. A MEMS gyroscope has small vibrating mass. When the sensor is rotated that mass experience a Coriolis force which displaces the vibrating mass from its original path. The gyroscope uses capacitance to sense this displacement and the output of proportional number of counts. If we rotate the gyroscope back and forth faster than the natural frequency, output will experience a drop in gain and some phase lag. Natural frequency will be in KHz range, gyroscopes are suggested to state bias and sensor noise. The state bias is the average output when the gyroscope is not rotating. The noise will be modelled as a band limited white noise; which means the noise has equal power at all frequencies.

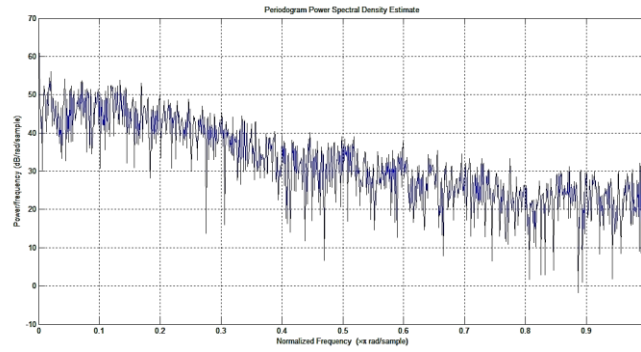


Fig. 8. Output of MEMS gyroscope dynamics

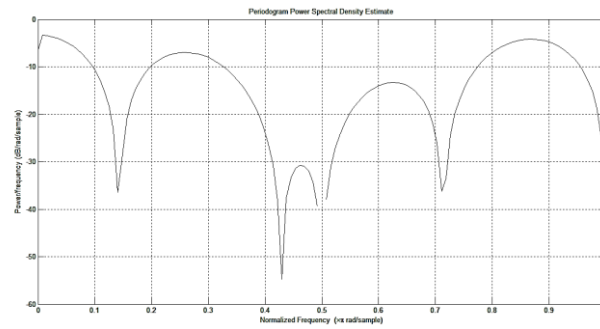
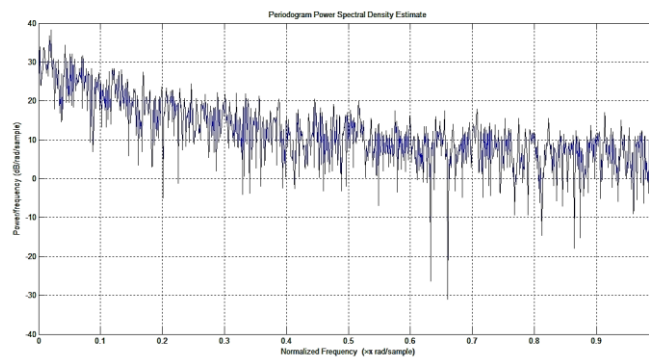
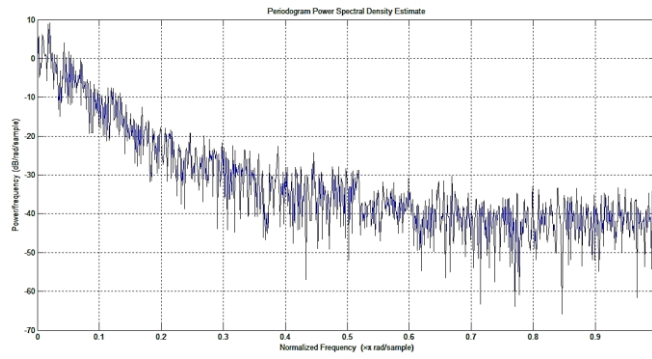


Fig. 9. Bitstream output of double closed-loop control system

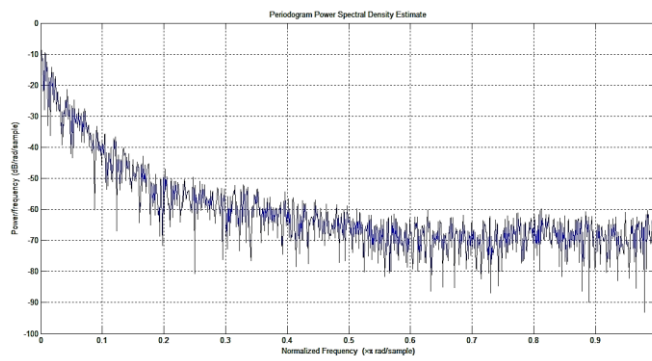
The model of L3GD20 has shown in fig. 11. The band limited noise and sensitivity of the gyroscope has obtained from the datasheet. It is embedded in the sense mode control-loop. The output of zero angular rate and bitstream output in power spectral density is shown and the signal-to-noise ratio has been calibrated.



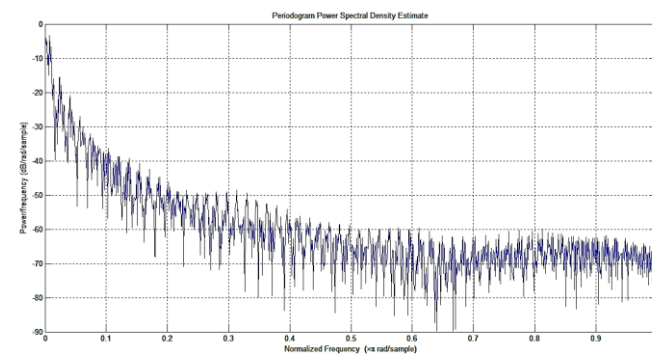
(a)



(b)



(c)



(d)

Fig. 10. (a) Output of resonator 1. (b) Output of resonator 2. (c) Output of resonator 3. (d) Output of resonator 4.

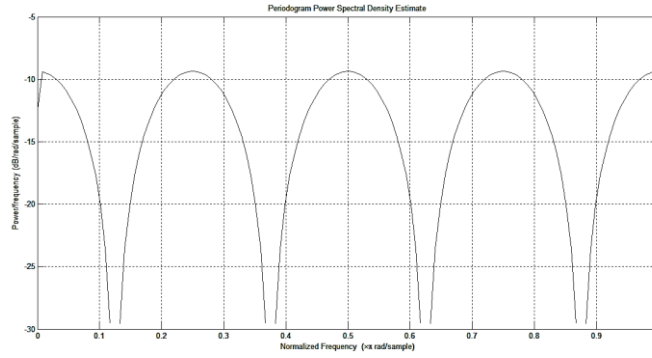


Fig. 13. Bitstream output of eighth-order sigma-delta modulator

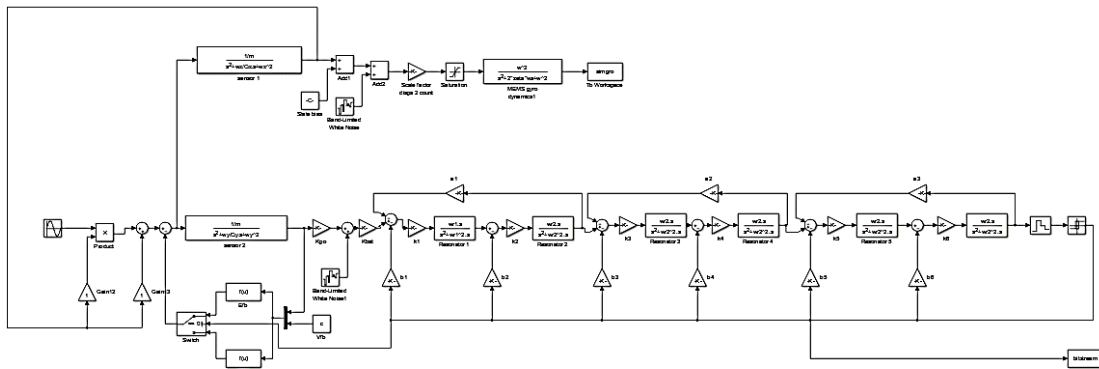
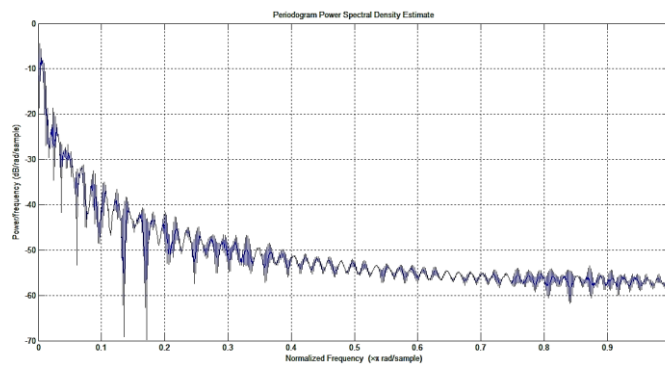
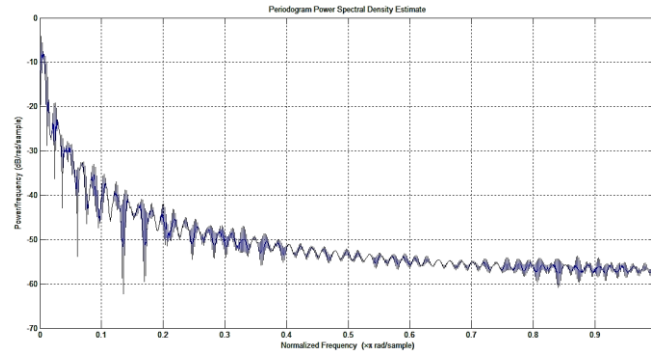


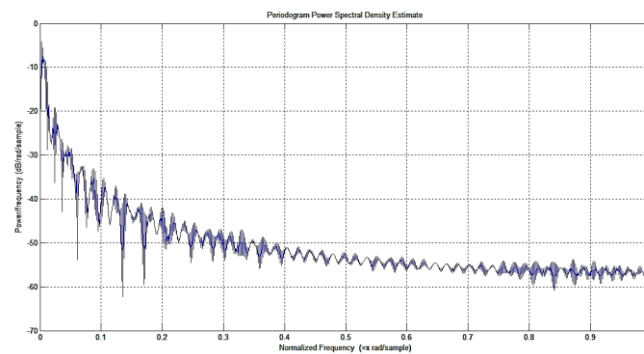
Fig. 14. Architecture of a closed loop control system controlled by an eight-order continuous-time force-feedback band-pass sigma-delta modulator



(a)



(b)



(c)

Fig. 15. Output of resonators 4,5 and 6

III. EXPERIMENTAL RESULTS AND FUTURE SCOPE

A double closed-loop control system has been implemented controlled by a sixth-order continuous-time force-feedback band-pass sigma-delta modulator. In fig. 3 topology of a sense mode control loop has shown. The architecture has been implemented using HRZ and RZ digital to analogue converter. Fig. 4 shows the output of the DAC, power spectral density (PSD) shows a deep notch in the output at 0.5rad/s; the magnitude ranges from -70dB to 50dB. At the drive mode frequency ω_x 4.304kHz; the magnitude is -50dB and at the sense mode frequency ω_y 4.338kHz; the magnitude is -98dB. In fig. 5 bitstream output is shown; for 0.425rad/s the magnitude is -55dB and for 0.46rad/s magnitude is -31dB. Force-feedback loop output is shown in fig. 6 and fig. 7 is the sensor output. Fig. 11 shows the model of the closed-loop control system without using HRZ and RZ DAC. Fig. 8 shows the output of zero angular rate input and fig. 9 is the bitstream output of the sense mode control loop. Fig. 10 shows the output of resonator1, resonator 2, resonator 3, resonator 4; in resonator 4, 0.65rad/s gives -90dB and 0.69rad/s gives -70dB. For 0.15rad/s it gives -60dB and 0.16rad/s gives -43dB. Fig. 12 shows the output of the sensor in the drive mode control loop. Fig. 14 shows the MATLAB Simulink model of an eighth-order continuous-time band-pass sigma-delta modulator. Fig. 13 shows the output bitstream; for 0.38rad/s it gives -29dB and for 0.5rad/s it gives -9dB. In

Fig. 15 (a) 0.15rad/s gives -70dB and 0.16rad/s gives -40dB; 0.65rad/s gives -55dB and 0.67rad/s gives -55dB. In fig. (b) 0.14rad/s gives -68dB and 0.15rad/s gives -42dB. In fig. (c) 0.14rad/s gives -62dB and 0.15rad/s gives -42dB.

The parameters can be optimized by using genetic algorithm (GA) and Monte Carlo simulation. The work describes about high-order and band-pass $\Sigma\Delta\text{M}$. The reason for using high-order and band-pass has discussed earlier. Hence future work can be done by implementing the architecture of eight-order continuous-time band-pass $\Sigma\Delta\text{M}$. Bandwidth can be maximized for better performance; the drive mode and sense mode should have a matching resonance frequency [15]. Structural imperfections reduced the performance of the device, resulting in a frequency of oscillation mismatch between two modes. This design could overcome the problems by adjusting the resonance frequency of both modes. For the autonomous control of phase and frequency, a phase locked loop (PLL) configuration can be implemented [16]. To generate a control signal for phase error regulation the phase difference between the drive and sense mode at the resonant frequency can be used.

III. CONCLUSION

This paper describes about the performance of MEMS vibratory gyroscope by using high-order band-pass sigma-delta modulator. Here we designed a sixth-order continuous-time band-pass sigma-delta modulator. It has been done in MATLAB Simulink. By selecting band-pass instead of low-pass only less sampling frequency is required and by choosing a high-order system, signal-to-noise ratio (SNR) and bandwidth has been increased and non-linearities has got reduced.

ACKNOWLEDGMENT

The authors wish to thank Y. Dong for the valuable discussions on high-order and low-order sigma-delta modulator.

REFERENCES

- [1] H. Xie, G. Feder, Integrated microelectromechanical gyroscopes, *J. Aerosp. Eng.*, vol.16, pp. 65-75, 2003.
- [2] R. Neul, et al., Micromachined angular rate sensors for automotive application, *IEEE J. sensors*, vol.7, pp.302-309, 2007.
- [3] V. P. Petkov, B. E. Boser, A fourth-order $\Sigma\Delta\text{M}$ interface for micromachined inertial sensors, *IEEE J. Solid-State circuits*, vol.40, pp.1602-1609, 2005.
- [4] V. P. Petkov, B. E. Boser, High-order electromechanical $\Sigma\Delta\text{M}$ modulation in micromachined inertial sensors, *IEEE Trans. Circuits Syst.-I*, vol.53, no.5, pp.1016-1022, 2006.
- [5] J. Raman, E. Cretu, P. Rombouts, L. Weyten, A digitally controlled MEMS gyroscope with unconstrained sigma-delta force-feedback architecture, in

- Proc. 19th IEEE Int. Conf. Micro Electro Mech. Syst., Istanbul, Turkey, 2006, pp. 710-713.
- [6] J. Raman, E. Cretu, P. Rombouts, L. Weyten, A closed-loop digitally controlled MEMS gyroscope with unconstrained sigma-delta force-feedback, *IEEE J. sensors*, vol.9, pp. 297-305, 2009.
- [7] H. Rodjegard, D. Sandstrom, P. Pelin, N. Hedenstierna, D. Eckerbert, G. I. Andersson, A digitally controlled MEMS gyroscope with 3.2 deg/Hr stability, 13th Conf. on Transducers'05, Seoul, Korea, 2005, pp. 535-538.
- [8] Y. Dong, M. Kraft, W. Redman-White, High order band-pass sigma delta interfaces for vibratory gyroscopes, in Proc. 4th IEEE Conf. Sensors, Irvine, USA, 2005, pp. 1080-1083.
- [9] Y. Dong, M. Kraft, W. Redman-White, Micromachined Vibratory gyroscopes controlled by a high-order band-pass sigma-delta modulator, *IEEE J. sensors*, vol.7, pp. 59-69, 2007.
- [10] Y. Dong, M. Kraft, W. Redman-White, 2007 High order noise shaping filters for high performance inertial sensors *IEEE Trans. Instrum. Measurement*, vol.56, pp. 1666-1674, 2007.
- [11] H. Ding, Z. Yang, G. Yan, M. Kraft, R. Wilcock, MEMS gyroscope control system using a band-pass continuous-time sigma-delta modulator, 9th IEEE Conf. Sensors, Hawaii, USA, 2010, pp. 868-872.
- [12] R. Maurino, P.Mole, A 200 MHz IF 11bit fourth-order bandpass sigma-delta ADC in SiGe, *IEEE J.Solid state Circuits*, vol.35, pp.959-967, 2000.
- [13] F. Chen, H. Chang, W. Yuan, R. Wilcock, M. Kraft, Parameter optimization for a high-order band-pass continuous-time sigma-delta modulator MEMS gyroscope using a genetic algorithm approach, *J. Micromech. Microeng*, vol.22 (105006), 2012.
- [14] R. Wilcock, M. Kraft, Genetic algorithm for the design of electro-mechanical Sigma Delta Modulator MEMS Sensors, *MDPI J. Sensors*, vol.10, pp.9217-9238, 2011.
- [15] Manut, MohdKharuddin, Zolkapli, Abdul Aziz, Design of MEMS gyroscope for wide range resonance frequency adjustment, in Proc. IEEE Int. Conf. Semiconductor Electronics (ICSE), Melaka, Malaysia, 2010, pp. 305-308.
- [16] Sangkyung Sung, Woon-Tahk Sung, Changjoo Kim, Sukchang Yun, and Young Jae Lee, On the mode-matched control of MEMS vibratory gyroscope via phase-domain analysis and design *IEEE Trans. Mechatronics*, vol.14, pp. 446-455, 2009.